

# Ultrahigh-Q photonic crystal cavities in silicon rich nitride

KAPIL DEBNATH,<sup>1,\*</sup> MARCO CLEMENTI,<sup>2</sup> THALÍA DOMÍNGUEZ BUCIO,<sup>1</sup> ALI Z. KHOKHAR,<sup>1</sup> MOÏSE SOTTO<sup>3</sup>, KATARZYNA M. GRABSKA,<sup>1</sup> DANIELE BAJONI,<sup>4</sup> MATTEO GALLI,<sup>2</sup> SHINICHI SAITO,<sup>3</sup> AND FREDRIC Y. GARDES<sup>1</sup>

<sup>1</sup>Optoelectronics Research Centre, University of Southampton, Southampton SO17 1BJ, UK

<sup>2</sup>Dipartimento di Fisica, Università di Pavia, via Bassi 6, 27100 Pavia, Italy

<sup>3</sup>Faculty of Physical Sciences and Engineering, University of Southampton, Southampton SO17 1BJ, UK

<sup>4</sup>Dipartimento di Ingegneria Industriale e dell'Informazione, Università di Pavia, via Ferrata 1, 27100 Pavia, Italy

\*K.Debnath@soton.ac.uk

**Abstract:** Ultrahigh-Q Photonic Crystal cavities were realized in a suspended Silicon Rich Nitride (SiNx) platform for applications at telecom wavelengths. Using a line width modulated cavity design we achieved a simulated Q of 520,000 with a modal volume of  $0.77(\lambda/n)^3$ . The fabricated cavities were measured using the resonance scattering technique and we demonstrated a measured Q of 120,000. The experimental spectra at different input power also indicate that the non-linear losses are negligible in this material platform.

© 2017 Optical Society of America

**OCIS codes:** (230.5298) Photonic crystals; (070.5753) Resonators; (130.0130) Integrated Optics.

---

## References and links

1. M. Notomi, "Manipulating light with strongly modulated photonic crystals," Rep. Prog. Phys. **73**(9), 096501 (2010).
2. B. S. Song, S. Noda, T. Asano, and Y. Akahane, "Ultra-high-Q photonic double-heterostructure nanocavity," Nat. Mat. **4**(3), 207-210 (2005).
3. E. Kuramochi, M. Notomi, S. Mitsugi, A. Shinya, T. Tanabe, and T. Watanabe, "Ultrahigh-Q photonic crystal nanocavities realized by the local width modulation of a line defect," Appl. Phys. Lett. **88**(4), 041112 (2006).
4. A. Simbula, M. Schatzl, L. Zagaglia, F. Alpeggiani, L. C. Andreani, F. Schäffler, T. Fromherz, M. Galli, and D. Gerace, "Realization of high-Q/V photonic crystal cavities defined by an effective Aubry-André-Harper bichromatic potential," APL Photon. **2**(5), 056102 (2017).
5. K. Debnath, K. Welna, M. Ferrera, K. Deasy, D. G. Lidzey, and L. O'Faolain, "Highly efficient optical filter based on vertically coupled photonic crystal cavity and bus waveguide," Opt. Lett. **38**(2), 154-156 (2013).
6. K. Debnath, L. O'Faolain, F. Y. Gardes, A. G. Steffan, G. T. Reed, and T. F. Krauss, "Cascaded modulator architecture for WDM applications," Opt. Exp. **20**(25), 27420-27428 (2012).
7. K. Debnath, F. Y. Gardes, A. P. Knights, G. T. Reed, T. F. Krauss, and L. O'Faolain, "Dielectric waveguide vertically coupled to all-silicon photodiodes operating at telecommunication wavelengths," Appl. Phys. Lett. **102**(17), 171106 (2013).
8. M. G. Scullion, A. Di Falco, and T. F. Krauss, "Slotted photonic crystal cavities with integrated microfluidics for biosensing applications," Biosens. Bioelectron. **27**(1), 101-105 (2011).
9. S. Azzini, D. Grassani, M. Galli, D. Gerace, M. Patrini, M. Liscidini, P. Velha, and D. Bajoni, "Stimulated and spontaneous four-wave mixing in silicon-on-insulator coupled photonic wire nano-cavities," Appl. Phys. Lett. **103**(3), 031117 (2013).
10. M. Galli, D. Gerace, K. Welna, T. F. Krauss, L. O'Faolain, G. Guizzetti, and L. C. Andreani, "Low-power continuous-wave generation of visible harmonics in silicon photonic crystal nanocavities," Opt. Exp. **18**(25), 26613-26624 (2010).
11. J. Upham, Y. Tanaka, Y. Kawamoto, Y. Sato, T. Nakamura, B. S. Song, T. Asano, and S. Noda, "Time-resolved catch and release of an optical pulse from a dynamic photonic crystal nanocavity," Opt. Exp. **19**(23), 23377-23385 (2011).
12. O. Painter, R. K. Lee, A. Scherer, A. Yariv, J. D. O'Brien, P. D. Dapkus, and I. Kim, "Two-dimensional photonic band-gap defect mode laser," Science **284**(5421), 1819-1821 (1999).
13. K. Hennessy, A. Badolato, M. Winger, D. Gerace, M. Atatüre, S. Gulde, S. Fält, E. L. Hu, and A. Imamoglu, "Quantum nature of a strongly coupled single quantum dot-cavity system," Nature **445**(7130), 896-899 (2007).
14. P. E. Barclay, K. Srinivasan, and O. Painter, "Nonlinear response of silicon photonic crystal microresonators excited via an integrated waveguide and fiber taper," Opt. Exp. **13**(3), 801-820 (2005).

15. L. D. Haret, T. Tanabe, E. Kuramochi, and M. Notomi, "Extremely low power optical bistability in silicon demonstrated using 1D photonic crystal nanocavity," *Opt. Exp.* **17**(23), 21108-21117 (2009).
16. C. Lacava, S. Stankovic, A. Z. Khokhar, T. D. Bucio, F. Y. Gardes, G. T. Reed, D. J. Richardson, and P. Petropoulos, "Si-rich silicon nitride for nonlinear signal processing applications," *Sci. Rep.* **7**(1), 22 (2017).
17. B. S. Song, S. Yamada, T. Asano, and S. Noda, "Demonstration of two-dimensional photonic crystals based on silicon carbide," *Opt. Exp.* **19**(12), 11084-11089 (2011).
18. W. H. Pernice, C. Xiong, C. Schuck, and H. X. Tang, "High-Q aluminum nitride photonic crystal nanobeam cavities," *Appl. Phys. Lett.* **100**(9), 091105 (2012).
19. M. Khan, T. Babinec, M. W. McCutcheon, P. Deotare, and M. Lončar, "Fabrication and characterization of high-quality-factor silicon nitride nanobeam cavities," *Opt. Lett.* **36**(3), 421-423 (2011).
20. D. Sam-Giao, D. Néel, S. Sergeant, B. Gayral, M. J. Rashid, F. Semon, J. Y. Duboz, M. Mexis, T. Guillet, C. Brimont, and S. David, "High quality factor AlN nanocavities embedded in a photonic crystal waveguide," *Appl. Phys. Lett.* **100**(19), 191104 (2012).
21. M. Barth, N. Nüsse, J. Stingl, B. Löchel, and O. Benson, "Emission properties of high-Q silicon nitride photonic crystal heterostructure cavities," *Appl. Phys. Lett.* **93**(2), 021112 (2008).
22. K. Debnath, T. D. Bucio, A. Al-Attili, A. Z. Khokhar, S. Saito, and F. Y. Gardes, "Photonic crystal waveguides on silicon rich nitride platform," *Opt. Exp.* **25**(4), 3214-3221 (2017).
23. T. Wang, D. K. T. Ng, S. K. Ng, Y. T. Toh, A. K. L. Chee, G. F. R. Chen, Q. Wang, and D. T. H. Tan, "Supercontinuum generation in bandgap engineered, back-end CMOS compatible silicon rich nitride waveguides," *Laser Photonics Rev.* **9**(5), 498-506 (2015).
24. D. K. T. Ng, Q. Wang, T. Wang, S. K. Ng, Y. T. Toh, K. P. Lim, Y. Yang, and D. T. H. Tan, "Exploring High Refractive Index Silicon-Rich Nitride Films by Low-Temperature Inductively Coupled Plasma Chemical Vapor Deposition and Applications for Integrated Waveguides," *ACS Appl. Mater. Interfaces* **7**(39), 21884-21889 (2015).
25. C. Krueckel, A. Fulop, T. Klintberg, J. Bengtsson, P. Andrekson, and V. Torres-Company, "Linear and nonlinear characterization of low-stress high-confinement silicon-rich nitride waveguides," *Opt. Express* **23**, 25827-25837 (2015).
26. T. D. Bucio, A. Z. Khokhar, C. Lacava, S. Stankovic, G. Z. Mashanovich, P. Petropoulos, and F. Y. Gardes, "Material and optical properties of low-temperature NH<sub>3</sub>-free PECVD SiN<sub>x</sub> layers for photonic applications," *J. Phys. D.: Appl. Phys.* **50**(2), 025106 (2017).
27. S. L. Portalupi, M. Galli, C. Reardon, T. F. Krauss, L. O'Faolain, L. C. Andreani, and D. Gerace, "Planar photonic crystal cavities with far-field optimization for high coupling efficiency and quality factor," *Opt. Express* **18**(15), 16064-16073 (2010).
28. M. Galli, S. L. Portalupi, M. Belotti, L. C. Andreani, L. O'Faolain, and T. F. Krauss, "Light scattering and Fano resonances in high-Q photonic crystal nanocavities," *Appl. Phys. Lett.* **94**(7), 071101 (2009).
29. The coupling efficiency is here defined as the ratio between the optical power coupled to the cavity mode and the total optical power incident on the cavity. As detailed in ref. [27], the peak intensity  $I$  of the resonant scattering spectrum is proportional to the light intensity that has been coupled to the cavity mode and reflected back to the detector in crossed polarizations. To normalize this quantity, we determine the intensity  $I_0$  of the incident light by replacing the sample with a nearly ideal dielectric mirror and measuring the reflected intensity, under the same focusing conditions but with parallel polarizations. Thus, we define the coupling efficiency as  $\eta_c = 8I/I_0$ . The factor 8 accounts for the double passage of light through the polarizer and analyser (see Fig. 2(a)) and the fact that only the backward resonant scattering signal is collected.
30. T. Carmon, L. Yang, and K. J. Vahala, "Dynamical thermal behavior and thermal self-stability of microcavities," *Opt. Express* **12**(20), 4742-4750 (2004).
31. Z. Yin, and F. W. Smith, "Optical dielectric function and infrared absorption of hydrogenated amorphous silicon nitride films: Experimental results and effective-medium-approximation analysis," *Phys. Rev. B* **42**(6), 3666-3672 (1990).
32. H. Mäkel, and R. Lüdemann, "Detailed study of the composition of hydrogenated SiN<sub>x</sub> layers for high-quality silicon surface passivation," *J. Appl. Phys.* **92**(5), 2602-2609 (2002).
33. S. K. Selvaraja, E. Sleetx, M. Schaeckers, W. Bogaerts, D. V. Thourhout, P. Dumon, and R. Baets, "Low-loss amorphous silicon-on-insulator technology for photonic integrated circuitry," *Opt. Comm.* **282**(9), 1767-1770 (2009).

## 1. Introduction

Two-dimensional Photonic Crystal (PhC) cavities have the ability to strongly confine light in both time and space [1]. Over the last decade, considerable amount of research has been devoted to realizing PhC cavities with ultra-high quality factors (Q) and with low mode volume (V) [2-4]. The unprecedentedly high Q/V values of such cavities offer several benefits for realizing compact optical devices with strong light-matter interaction, which can be orders of magnitude higher than the corresponding bulk medium. High-Q PhC cavities have been exploited for diverse fields of application, such as, in integrated photonics for optical filters, modulators, detectors [5-7]; for sensing applications [8]; in nonlinear photonics for four-wave mixing [9]

and harmonic generation [10]; for optical pulse manipulation [11]; for low-threshold lasers [12]; for cavity quantum electrodynamics [13] and many more. In the past, although many clever PhC cavity designs have been proposed and demonstrated to show remarkably high Q-factors, the choice of material platform has mainly been limited to high refractive index contrast materials, such as silicon (Si) or gallium arsenide (GaAs). Particularly, for its mature fabrication process and potential monolithic opto-electronic integration, Si has become the most preferred material for demonstrating optical devices with PhC cavities with ultra-high Q-factors for telecom wavelengths. However, for many applications that require high optical power, such as nonlinear photonics, silicon imposes a fundamental limitation due to its prohibitively high two-photon absorption (TPA). High-Q cavities just enhance such nonlinear absorption due to strong optical confinement. For example, TPA and associated free carrier absorption (FCA) becomes significant in PhC cavities at an input power level as low as few  $\mu$ Ws [14, 15]. Very recently, wide bandgap materials, such as Aluminium Nitride (AlN), Silicon Carbide (SiC), and Silicon Nitride ( $\text{Si}_3\text{N}_4$ ) are gaining interest due to their negligible TPA, better thermal and mechanical properties, and also broadband operation covering telecom to visible wavelengths [16, 17]. Although, 1D nanobeam cavities with high Q-cavities have been demonstrated in these platforms [18, 19], 2D PhC cavities with high Q-factors have not yet been realized. Due to their relatively low refractive index contrast, previously demonstrated Q-factors were only limited to few thousands [20, 21]. In this letter, we report 2D cavities with Q-factors over 120,000 in air membraned silicon rich nitride ( $\text{SiNx}$ ) platform. We have previously demonstrated PhC waveguides with low propagation loss and high group index in this  $\text{SiNx}$  platform [22].  $\text{SiNx}$  offers several advantages: i) Unlike stoichiometric  $\text{Si}_3\text{N}_4$ , the refractive index can be optimized for specific applications by controlling the Si concentration, ii) the nonlinear Kerr coefficient can be improved significantly, comparable to bulk Si, with negligible TPA, iii) CMOS compatible fabrication process with possibility of 3D integration [16, 23-25].

## 2. Design and Fabrication

For this demonstration we used a well-known line-width modulated 2D PhC cavity design, first proposed by Kuramochi et al. [3]. The cavity was formed in a hexagonal PhC lattice of air holes in a 300 nm thick  $\text{SiNx}$  slab. The lattice period and air hole radius of the background PhC was chosen to be  $a = 570$  nm and  $r = 0.30a$ , so that the resonance wavelengths of the cavities could fall within the telecom wavelength range. The cavity was defined in a W1 waveguide with its axis along  $\Gamma$ -K direction. The optical confinement was achieved by shifting a set of air holes away from the center of the waveguide. In Fig. 1(a), the holes in red, yellow and purple are shifted along the y-direction by  $\Delta A$  (y),  $\Delta B$  ( $= \frac{2}{3}y$ ) and  $\Delta C$  ( $= \frac{1}{3}y$ ) respectively. For calculating the Q-factors and resonance wavelengths we used the 3D finite-difference-time-domain (FDTD) method. The calculation area was set to 55 periods along the x-axis, 22 periods along the y-axis and  $2 \mu\text{m}$  along the z-axis. The minimum mesh size was chosen to be  $0.02a_x$ ,  $0.02a_y$ , and 30 nm along x, y and z directions respectively. Using these simulation parameters, we have optimized the cavity design by varying the hole shifts. We changed the value of y from 3 nm up to 21 nm and achieved the highest Q-factor of 520,000 with resonance wavelength at 1569 nm for  $y = 12$  nm. The modal volume of the cavity with  $y = 12$  nm was calculated to be  $0.77(\lambda/n)^3$ . Such high Q-factor with low modal volume implies that it is possible to achieve optical performance comparable to conventional Si based PhC cavities in  $\text{SiNx}$ . Figure 1(b) shows the simulated dominant electric field ( $|E_y|$ ) profile of the resonant mode. The optical mode is strongly confined near the center of the cavity and gradually attenuates away from the center.

To confirm the calculated optical properties of the designed PhC cavities, the devices were fabricated in a  $\text{SiNx}$ -on-Si substrate. A 300 nm thick layer of  $\text{SiNx}$  was first deposited on a 6-inch Si wafer with (100) surface orientation using plasma enhanced chemical vapor deposition (PECVD) system. The details of the deposition recipe and its optimization can be found in our

previously reported work [22, 26]. From the ellipsometry data we found that the refractive index of the deposited SiN<sub>x</sub> was 2.48 at 1550 nm wavelength. The wafer was then spin coated with a 450 nm thick layer of e-beam resist ZEP 520A. Using e-beam lithography, the PhC cavity patterns were exposed into the ZEP layer. After developing the exposed resist using ZED-N50, the PhC cavity patterns were transferred into the SiN<sub>x</sub> layer in an inductively coupled plasma (ICP) system using SF<sub>6</sub>/CHF<sub>3</sub> gas chemistry. After removing the left over resist, the wafer was immersed in a 25% aqueous solution of Tetra-methyl-ammonium hydroxide (TMAH). TMAH selectively etched away the bottom Si through the exposed areas leaving the SiN<sub>x</sub> layer with PhC cavity regions suspended. Figure 1(c) shows an SEM image of the fabricated PhC cavity. The hole shifts were too small to be distinguished visually. Figure 1(d) shows the cross-sectional view of the suspended PhC structure. A zoomed in view of the PhC region, shown in the inset of Fig. 1(d), reveals some surface roughness, which we believe comes from the deposition process and according to atomic force microscopy (AFM) the roughness was around 4 nm (rms).

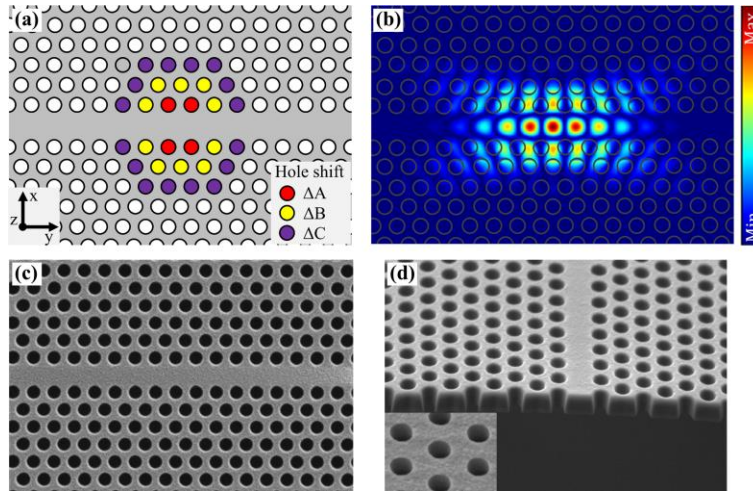


Fig. 1. (a) Schematic of the PhC cavity design by line width modulation [3]. The cavity is defined in a W1 PhC cavity by shifting several holes away from the center of the waveguide. The holes in red, yellow and purple are shifted along y-direction by  $\Delta A$  ( $y$ ),  $\Delta B$  ( $= \frac{2}{3}y$ ) and  $\Delta C$  ( $= \frac{1}{3}y$ ) respectively. (b) Simulated dominant electric field ( $|E_y|$ ) profile of the cavity resonant mode for  $y = 12$  nm. (c) SEM image of the fabricated PhC cavity. The hole shifts were too small to be distinguished visually. (d) SEM image showing the cross-section of the suspended PhC structure. The inset shows a zoomed in view of the structure. Surface roughness due to the deposition process is visible at this scale.

### 3. Characterization

The cavities were characterized at room temperature ( $T = 300$  K) using the resonant scattering (RS) technique. The setup is shown in Fig. 2(a) and a detailed discussion about the technique can be found in [27]. In short, in this technique, the continuous-wave laser light scattered from the PhC cavities was measured using a crossed-polarization setup consisting of a polarizer and analyser. To achieve a high signal-to-noise ratio, the cavity is oriented at  $45^\circ$  with respect to the axis of the polarizer and analyser, thus maximising the resonant signal over the background reflection. The advantage of using the RS technique is that, unlike in-plane characterization methods that use coupling waveguides [3], RS spectrum directly gives the intrinsic Q-factor of the cavity and also offers high signal-to-noise ratio. We achieved experimentally the highest Q-factor for the cavity with  $y = 6$  nm. Figure 2(b) shows the RS spectrum of the same cavity around its resonance wavelength at 1558.59 nm. The red dots represent the measured RS signal and the black line indicates a Fano-fit to determine the linewidth of the resonance peak. The reason for using a Fano-fit instead of a Lorentzian fit is because occasionally a Lorentzian

spectrum can become asymmetric due to different coupling conditions into the cavity. This asymmetry arises from the Fano interference between the scattering due to the cavity resonance (discrete state) and the scattered light from the background PhC (continuum of states) [28]. We estimated the Q-factor of the cavity from the linewidth of the best fit of the resonance peak with a Fano function (black line). An extremely narrow linewidth of ~13 pm corresponding to a Q-factor of 122,000 was obtained.

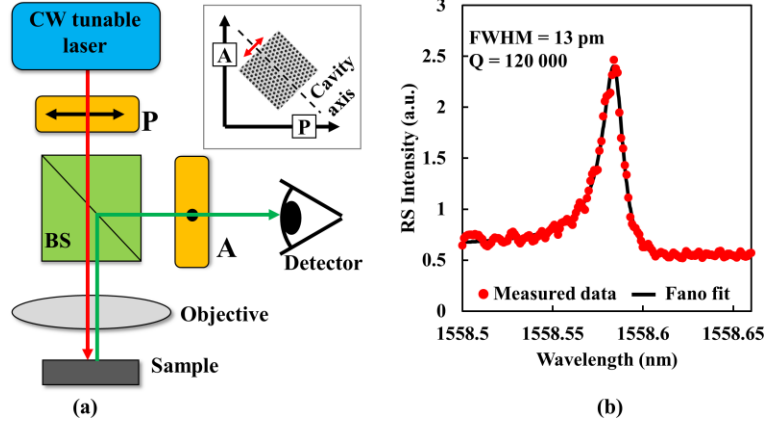


Fig. 2. (a) A schematic of the resonance scattering setup, the inset shows the orientation of the PhC cavity with respect to the axis of the polarizer and analyzer. (b) Measured RS spectrum around the resonance wavelength for the PhC cavity with  $y = 6$  nm.

Figure 3 compares the simulated and measured Q-factors and resonance wavelengths as functions of the hole shifts ( $y$ ). In Fig. 3(a) the experimentally determined Q-factors were plotted using red circles, while the simulated values are shown by blue diamonds. For  $y = 12$  nm, we achieved the highest simulated Q-factor of 520,000 and for other values of  $y$ , the Q-factor drops monotonically away from  $y = 12$  nm. For measurements, the signal strength from the RS setup depends on the refractive index contrast of the material and the strength of the disorder in the structure. For our low index SiNx PhC cavities the signal strength was relatively poor compared to Si based PhC cavities. As a result we could not successfully measure the cavity spectrum from the device with  $y = 3$  nm. For the rest of the cavities with  $y$  varying from 6 nm to 21 nm, the Q-factor varied between 71,000 and 122,000. Although we observed a clear trend in the simulated result with highest Q-factor for the cavity with  $y=12$  nm, the experimental values do not follow any such trend. We believe this variation is within the limit of statistical uncertainty due to the fabrication process. Also, we notice that the highest measured Q-factor is limited by the Q-factor associated with the material loss and fabrication. Ref [16] reports a propagation loss of 1.5 dB/cm for waveguides fabricated using the same material and similar fabrication process. From this loss value we can roughly estimate the Q-factor associated with the material loss and fabrication using the formula  $Q = 2\pi n / \lambda \alpha$ , where  $n$  is the refractive index of SiNx around wavelength  $\lambda$  of 1.55  $\mu\text{m}$  and  $\alpha$  is the propagation loss (in  $\mu\text{m}^{-1}$ ). According to this equation, our cavity Q-factors are limited to 145,000. This is highlighted using the grey dashed line in Fig. 3(a). Figure 3(b) shows how the resonance wavelength red-shifts as a function of hole shift. The simulated values are shown in green circles, whereas the measured values are shown in yellow squares. From the simulated values, the optical resonance is at 1562 nm for the cavity with  $y = 3$  nm while the resonance wavelength shifts to 1572 nm for the cavity with  $y = 21$  nm, i.e., by more than 10 nm. For most of the cavities we found a good agreement between the experimental results and the simulated results.

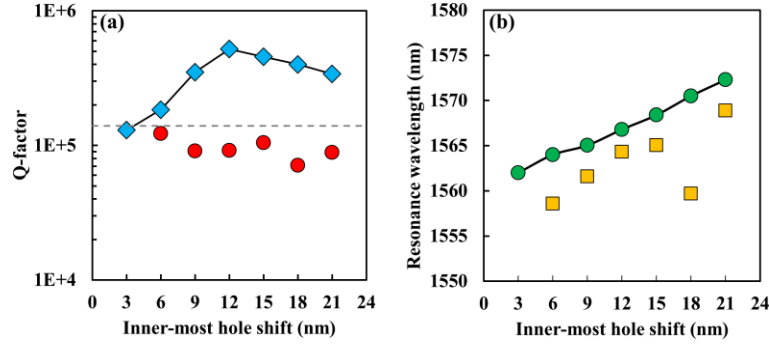


Fig. 3. (a) Cavity Q-factors as a function of inner-most hole shift ( $y$ ). Blue diamonds represents the simulated Q values and red circles represent the measured Q- values. (b) Cavity resonance wavelengths as a function of inner-most hole shift ( $y$ ). Green circles represents the simulated resonance wavelengths and yellow squares represent the measured resonance wavelengths.

Finally, we characterized our cavities at different input powers. We swept the CW laser light from shorter to longer wavelengths and measured the RS signal. Figure 4(a) shows the RS intensity spectrum of the cavity with  $y = 12$  nm for different coupled power. Our coupling efficiency was about 6% [29]. For low input powers, the cavity spectrum shown a Fano shape similar to the one reported in Fig. 3(b); however, as the input power increased, the shape of the RS spectrum dramatically changed to an asymmetric saw-tooth shape. This resulted from a well-known phenomenon of thermally induced optical bistability [14, 15, 30]. For a fixed input power, as the input light starts to couple into the cavity, the cavity temperature starts to rise due to linear and nonlinear absorptions causing a red-shift in the resonance wavelength from the cold cavity resonance (in this case at 1564.29nm) and due to a positive feedback between the laser red-sweeping and cavity resonance red-shift the RS spectrum broadens. However, when the detuning becomes too large for the cavity to follow, the RS intensity drops sharply to zero, indicating that the bistable state exists. In this cavity, the evidence of strong optical bistability was visible at a coupled power as low as 5.66  $\mu$ W. As the input power increased, the effect of bistability also becomes more prominent and the wavelength where the transition happens also red-shifts, which is the new resonance wavelength of the hot cavity. There are various absorption mechanisms which could cause a change in the cavity temperature leading to a change in refractive index due to thermo-optic effect: linear absorption, FCA and TPA [14, 15]. One way to identify the effect of the different absorption mechanisms on the cavity behaviour is by observing the shift in resonance wavelength with increasing input power. Therefore, in Fig. 4(b) we plotted the resonance wavelength as a function of the coupled optical power. Interestingly, the shift in resonance wavelength is linear for a change in coupled power over three orders of magnitude from 0.340  $\mu$ W up to 180  $\mu$ W. This suggests that nonlinear absorption losses, especially TPA or TPA related FCA (which are significantly prominent in Si based PhC cavities [14, 15]), are negligible within the power level of our measurement. Also, since the SiNx layer was deposited using PECVD we do not expect any direct FCA due to the presence of free carriers [26]. We notice that a more detailed analysis of the nonlinear response of our PhC cavities using a theoretical model for linear and nonlinear absorption processes would require the knowledge of important material parameters such as the thermal conductivity and specific heat, which are still object of investigation for this new SiNx material. The main source of bistability in our cavities is the intrinsic linear absorption of the material platform. There are several sources that can be responsible for such absorption in our deposited SiNx layer. Si rich layers as ours have shown an increased amount of Si-H and Si-Si bonds due to their increased Si content [26]. The presence of Si-H bonds produces vibrational overtones with energy absorption tails extended over the telecom wavelengths around 1550nm that can increase the intrinsic loss of the material [31]. Moreover, the high concentrations of Si-H and Si-Si bonds can lead to the formation undesired Si dangling bonds and material defects such as grains,

pores, voids and surface roughness (see inset in Fig. 1(d)) that can produce additional scattering and absorption losses [32, 33].

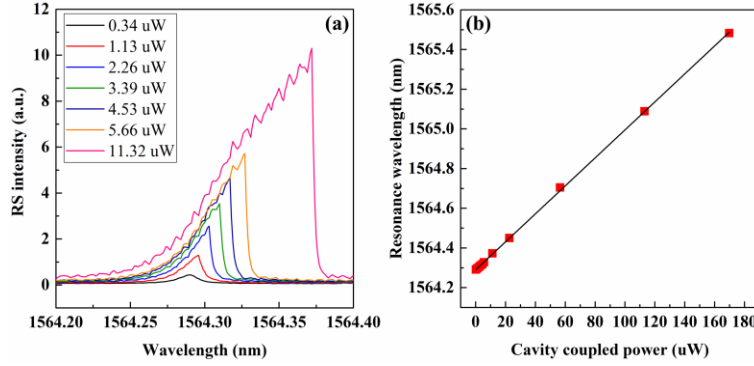


Fig. 4. (a) RS spectrum of the cavity with  $y= 12$  nm for different coupled powers showing characteristic bistability line shape. (b) Plot of resonance wavelength as a function of coupled power showing a clear linear relationship.

#### 4. Conclusion

In conclusion, we have experimentally demonstrated ultra-high Q PhC cavities in a low refractive index contrast SiNx/air material platform. For this demonstration we used a line width modulated cavity design. Initial numerical results suggested a Q-value of over  $5 \times 10^5$  could be achieved with such cavity design. Experimentally, we achieved a Q value of as high as 122,000; this was mainly limited by the material loss and fabrication loss of the platform. The bistability measurement of these cavities reveal that there are no nonlinear losses, such as TPA or FCA, present in these cavities even for a coupled power as high as  $180 \mu\text{W}$ . Ultra-high Q-values associated with no nonlinear loss makes these cavities a very promising structure for nonlinear photonic applications.

#### Funding

This work was supported by the H2020 project COSMICC (688516), EPSRC Standard Grant (EP/M009416/1), EPSRC Manufacturing Fellowship (EP/M008975/1), EPSRC Platform Grant (EP/N013247/1), and EU FP7 Marie-Curie Carrier-Integration-Grant (PCIG13-GA-2013-618116). EPSRC Standard Grant HERMES (EP/K02423X/1), EPSRC Standard Grant CORNERSTONE (EP/L021129/1). All data supporting this study are available from the University of Southampton repository at: <http://doi.org/10.5258/SOTON/D0212>.